

ELECTROMAGNETIC SCATTERING BY MULTI-WALL CARBON NANOTUBES

S. M. Mikki

Electrical Engineering Department
Royal Military College, Canada

A. A. Kishk

Department of Electrical Engineering
University of Mississippi
USA

Abstract—We provide here a theoretical description of electromagnetic scattering by multi-wall carbon nanotubes based on an effective-boundary condition derived previously using a phenomenological quantum model. We present the basic analytical solution, extending it then to include the electromagnetic interaction between multiple concentric tubes in the general multi-wall carbon nanotube case.

1. INTRODUCTION

Carbon nanotubes (CNTs), first reported in [1], are crystal structures in the form of single (or multiple co-centric) cylindrical tubes with high aspect ratio. They have been proposed as candidates for various applications, ranging from enhancement of the mechanical properties of composites to logical gates in new genre of nano-electronic devices [2, 3]. The fact that they can function as either metallic or semiconducting, depending on the geometric structures, has attracted the attention of many researchers to systematically investigate their performance under wide range of conditions. Among the most important classes of interactions that has been in the focus in recent years is the response of the nanotube to external electromagnetic fields. The present work is an extension of an electromagnetic scattering model proposed by the authors for single-wall CNTs [8].

Corresponding author: S. M. Mikki (makkisaid@hotmail.com).

Here, we provide a theoretical description of the electromagnetic scattering by *multi*-wall carbon nanotubes based on an effective-boundary condition derived previously using a phenomenological quantum model [5, 6]. The analytical solution for the scattering problem developed by the authors in [8] was compared with experiments and good results had been obtained. The fundamental assumption invoked in the present paper is that the inter-layer tube interaction leads to no significant changes in the quantum model derived in [5] and [6] for single-wall CNTs. In this case, the quantum model can be applied to describe the boundary condition on each wall independently. Our goal in this paper is to derive the electromagnetic interaction for an arbitrary multi-wall CNT based on this assumption.

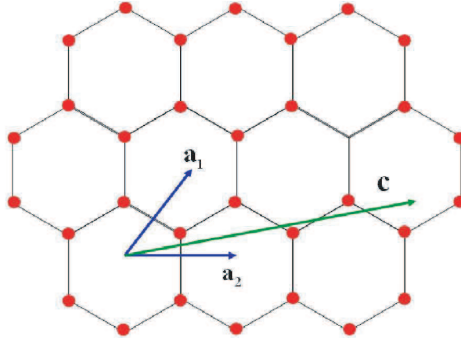


Figure 1. Graphene sheet used in forming a CNT. The dots illustrate the positions of carbon atoms.

2. REVIEW OF THE STRUCTURE OF CARBON NANOTUBES

Figure 1 illustrates the honeycomb lattice structure of graphene[†]. The unit cell is specified by two atoms located at the positions $1/3(\mathbf{a}_1 + \mathbf{a}_2)$ and $2/3(\mathbf{a}_1 + \mathbf{a}_2)$, where \mathbf{a}_1 and \mathbf{a}_2 are two unit vectors defining the lattice constants and $b_0 = |\mathbf{a}_1| = |\mathbf{a}_2| = 0.142 \text{ nm}$ is the interatomic distance. The CNT is formed by rolling up this sheet such that the circumference of the tube coincides with the chiral vector $\mathbf{c} = m\mathbf{a}_1 + n\mathbf{a}_2$. Here m and n are two integers that completely

[†] Graphene is defined as a 2D layer of graphite.

determine the structure and the properties of the CNT. If only one layer is used to form the tube, the resulting structure is called single-wall CNT (SWCNT). Alternatively, if the tube consists of several concentric cylinders, we call it multi-wall CNT (MWCNT). CNTs with the structure $(n, 0)$ are called *zig-zag* CNT because the pattern created along the circumference of the tube resembles a zig-zag motion. The structure (n, n) is called *armchair*. Tubes that have $0 < n \neq m$ are called *chiral*. The radius of the CNT is given by [2]

$$b = \frac{|\mathbf{c}|}{2\pi} = \frac{b_0}{2\pi} \sqrt{m^2 + mn + n^2}. \quad (1)$$

One of the most important features of CNTs is their ability to manifest in different transport modes depending on the geometry, which is completely specified by the integers m and n . Armchair CNTs are always metallic since the resulting energy diagram has no energy bandgap. Zig-zag tubes can be either metallic or semiconducting depending on the chirality (i.e., the ratio m/n). If $m = 3i$, where i is an integer, then the resulting CNT will be metallic. Otherwise, a non-zero bandgap will exist and the properties of the structure becomes closer to semiconductors.

3. THE EFFECTIVE-BOUNDARY CONDITION

In CNTs, the so-called π -electron, which belongs to an unsaturated orbital orthogonal to the tube surface, is relatively free and can therefore respond to an external electromagnetic fields [2]. The interaction of this electron with external electromagnetic field leads to postulating an effective conductivity function describing the current induced by the interaction. The idea of the effective-boundary condition is to replace a microscopic fine crystal structure of matter, in this case the carbon nanotube atomic lattice arranged in a cylindrical fashion, by an effective, homogenized surface in which the behavior of the electromagnetic field on the two sides of the surface can be described by formulas familiar to conventional macroscopic electromagnetism, e.g., boundary conditions.

The effective-boundary condition is given by [6]

$$\hat{n} \times (\mathbf{E}^1 - \mathbf{E}^2) = 0, \quad (2)$$

$$\hat{n} \times (\mathbf{H}_z^1 - \mathbf{H}_z^2) = 0, \quad (3)$$

$$\{1 + \Upsilon(\omega) \partial^2 / \partial z^2\} \hat{n} \times (\mathbf{H}_\varphi^2 - \mathbf{H}_\varphi^1) = \sigma_{\text{cn}}(\omega) (\hat{z} \cdot \mathbf{E}) \hat{z}, \quad (4)$$

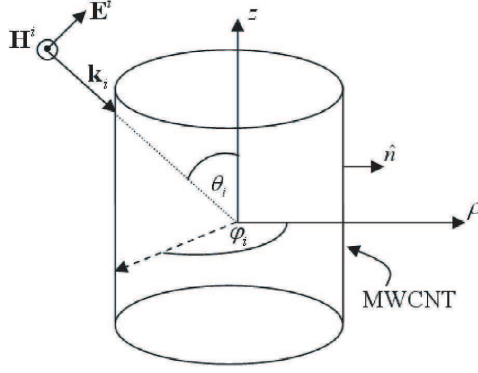


Figure 2. Scattering of the TM^z mode by MWCNT.

where the unit normal vector \hat{n} is directed as shown in Figure 2. The field components indexed by 1 and 2 refer to the fields in the inside and outside regions, respectively. Here, $\Upsilon(\omega)$ represents the effect of spatial dispersion in the z -direction and is given by

$$\Upsilon(\omega) = l_0 / [(\omega/c)(1 - j/\omega\tau)], \quad (5)$$

where, l_0 is estimated to be around 10^{-5} for metallic tubes [6].

The azimuthal current of the CNT is very weak compared to the axial component and therefore is ignored in the boundary conditions above. The axial conductivity for armchair CNT is given by [5, 6]

$$\sigma_{\text{cn}}(\omega) = \frac{j e^2 \omega}{\pi^2 \hbar \rho_{\text{cn}}} \left\{ \frac{1}{\omega(\omega - j\nu)} \sum_{s=1}^m \int dp_z \frac{\partial F_c}{\partial p_z} \frac{\partial \mathcal{E}_c}{\partial p_z} + 2 \sum_{s=1}^m \int dp_z \mathcal{E}_c |R_{vc}|^2 \frac{F_c - F_v}{\hbar^2 \omega(\omega - j\nu) - 4\mathcal{E}_c^2} \right\}, \quad (6)$$

where ν is the *relaxation frequency*, which is related to the *relaxation time* τ by $\nu = \tau^{-1}$. The normalized Planck's constant is given by $\hbar \approx 1.05457 \times 10^{-34}$ J·s and the electron charge $e \approx 1.6022 \times 10^{-19}$ C. The dispersion relation of CNTs is a well-known function given by

$$\mathcal{E}_{c,v}(p_z, s) = \pm \gamma_0 \sqrt{1 + 4 \cos\left(\frac{\pi s}{m}\right) \cos\left(\frac{d}{\sqrt{3}} p_z\right) + 4 \cos^2\left(\frac{d}{\sqrt{3}} p_z\right)}, \quad (7)$$

where p_z is the quasi-momentum in the z -direction, $\mathcal{E}_{c,v}$ is the energy level in the conduction/valence band, $d = 3a_0/2\hbar$, and the positive

and negative signs in (7) corresponds to the conduction and valence bands, respectively. The equilibrium Fermi-Dirac distribution for the conduction and valence bands can be calculated by

$$F_{c,v} = \frac{1}{1 + \exp(\mathcal{E}_c/k_B T)}, \quad (8)$$

where $k_B = 1.381 \times 10^{-23}$ J/K is Boltzmann's constant and T is the absolute temperature. The matrix element for armchair CNT is given by

$$R_{vc}(p_z, s) = \frac{\sqrt{3}a_0\gamma_0^2}{2\mathcal{E}_c^2} \sin\left(\frac{d}{\sqrt{3}}p_z\right) \sin\left(\frac{\pi s}{m}\right). \quad (9)$$

The integrals in (6) are calculated in the first Brillouin zone. One possible zone is the integrations limits $p_z = \pm 2\pi\hbar/\sqrt{3}a_0$. The numerical cost for calculating the quantum conductivity (6) increases dramatically with large m .

4. GENERAL CONSIDERATIONS

We start from the vector wave equation in homogenous medium

$$\nabla \times \nabla \times \mathbf{E} - k^2 \mathbf{E} = 0, \quad \nabla \times \nabla \times \mathbf{H} - k^2 \mathbf{H} = 0, \quad (10)$$

where $k = \omega/c$. In cylindrical coordinates, using the vector identity $\nabla \times \nabla \times \mathbf{A} = \nabla \nabla \cdot \mathbf{A} - \nabla^2 \mathbf{A}$, Equation (10) becomes

$$\nabla^2 \mathbf{E} + k^2 \mathbf{E} = 0, \quad \nabla^2 \mathbf{H} + k^2 \mathbf{H} = 0, \quad (11)$$

where we have used the fact that $\nabla \cdot \mathbf{E} = \nabla \cdot \mathbf{H} = 0$ in source-free region. In cylindrical coordinates, only the z -components satisfy the scalar Helmholtz equations

$$(\nabla^2 + k^2) E_z = 0, \quad (\nabla^2 + k^2) H_z = 0. \quad (12)$$

The general solution of Equation (3) is given by

$$\begin{pmatrix} E_z \\ H_z \end{pmatrix} = \left[\mathbf{A}_n J_n(k_\rho \rho) + \mathbf{B}_n H_n^{(2)}(k_\rho \rho) \right] F_n(z), \quad (13)$$

where $k_\rho = \sqrt{k^2 - k_z^2}$ and \mathbf{A}_n and \mathbf{B}_n are some constant vectors. Here we have

$$F_n(z) = e^{-jk_z z - jn\varphi}. \quad (14)$$

The transverse fields are found by [10]

$$E_t = \frac{1}{k_\rho^2} [-jk_z \nabla_t E_z + j\omega\mu\hat{z} \times \nabla_t H_z] \quad (15)$$

and

$$H_t = \frac{1}{k_\rho^2} [-jk_z \nabla_t H_z + j\omega\varepsilon\hat{z} \times \nabla_t E_z], \quad (16)$$

where the transverse dell operator is given by

$$\nabla_t = \hat{\rho} \frac{\partial}{\partial \rho} + \hat{\varphi} \frac{1}{\rho} \frac{\partial}{\partial \varphi} = \hat{\rho} \frac{\partial}{\partial \rho} - \hat{\varphi} \frac{jn}{\rho}. \quad (17)$$

5. CANONICAL SOLUTION FOR SINGLE-WALL CARBON NANOTUBES

We provide first the kernel of our solution, which consists of two canonical cases, the standing and outgoing wave of a SWCNT. Once we know how the nanotube behaves in these two cases, the response to arbitrary source excitation can be determined by using the Fourier integral theorem.

5.1. Standing Wave Problem

Consider Figure 3(a) where we assume that a standing wave is incident on the SWCNT. The fields in region 2 (outer region) consists of the

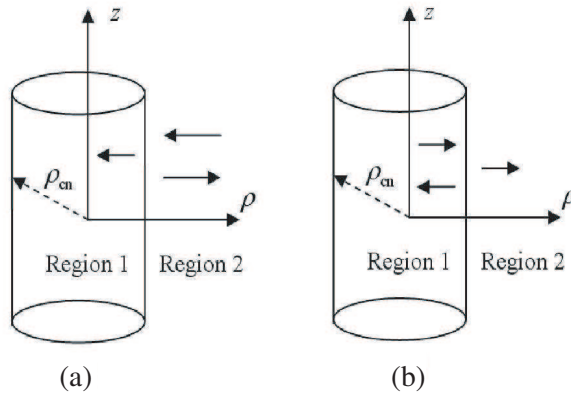


Figure 3. Scattering of incident waves by SWCNT (a) standing wave, (b) outgoing wave.

direct wave plus scattered part. The total field is given by

$$\begin{pmatrix} E_{2z} \\ H_{2z} \end{pmatrix} = J_n(k_\rho\rho) F_n(z) \mathbf{a}_2 + H_n^{(2)}(k_\rho\rho) F_n(z) \bar{\mathbf{R}}_{21} \cdot \mathbf{a}_2, \quad (18)$$

The fields in region 1 (inner region) are given by

$$\begin{pmatrix} E_{1z} \\ H_{1z} \end{pmatrix} = J_n(k_\rho\rho) F_n(z) \bar{\mathbf{T}}_{21} \cdot \mathbf{a}_2, \quad (19)$$

where $\bar{\mathbf{R}}_{21}$ and $\bar{\mathbf{T}}_{21}$ are the reflection and transmission matrices, respectively. Applying (18) and (19) into (15) and (16), we find

$$\begin{pmatrix} H_{2\varphi} \\ E_{2\varphi} \end{pmatrix} = \bar{\mathbf{J}}_n(k_\rho\rho) \cdot \mathbf{a}_2 F_n(z) + \bar{\mathbf{H}}_n^{(2)}(k_\rho\rho) \cdot \bar{\mathbf{R}}_{21} \cdot \mathbf{a}_2 F_n(z) \quad (20)$$

and

$$\begin{pmatrix} H_{1\varphi} \\ E_{1\varphi} \end{pmatrix} = \bar{\mathbf{J}}_n(k_\rho\rho) \cdot \bar{\mathbf{T}}_{21} \cdot \mathbf{a}_2 F_n(z), \quad (21)$$

where

$$\bar{\mathbf{J}}_n(k_\rho\rho) = \frac{1}{k_\rho^2\rho} \begin{pmatrix} -j\omega\varepsilon k_\rho\rho J_n'(k_\rho\rho) & -nk_z J_n(k_\rho\rho) \\ -nk_z J_n(k_\rho\rho) & j\omega\mu k_\rho\rho J_n'(k_\rho\rho) \end{pmatrix} \quad (22)$$

and

$$\bar{\mathbf{H}}_n(k_\rho\rho) = \frac{1}{k_\rho^2\rho} \begin{pmatrix} -j\omega\varepsilon k_\rho\rho H_n'(k_\rho\rho) & -nk_z H_n(k_\rho\rho) \\ -nk_z H_n(k_\rho\rho) & j\omega\mu k_\rho\rho H_n'(k_\rho\rho) \end{pmatrix}. \quad (23)$$

Applying the boundary conditions (2) and (4), we find

$$\begin{aligned} & J_n(k_\rho\rho_{cn}) F_n(z) \mathbf{a}_2 + H_n^{(2)}(k_\rho\rho_{cn}) F_n(z) \bar{\mathbf{R}}_{21} \cdot \mathbf{a}_2 \\ & = J_n(k_\rho\rho_{cn}) F_n(z) \bar{\mathbf{T}}_{21} \cdot \mathbf{a}_2 \end{aligned} \quad (24)$$

and

$$\begin{aligned} & (1 - \Upsilon(\omega) k_z^2) F_n(z) \bar{\mathbf{J}}_n(k_\rho\rho_{cn}) \cdot \mathbf{a}_2 \\ & + \bar{\mathbf{H}}_n^{(2)}(k_\rho\rho_{cn}) \cdot \bar{\mathbf{R}}_{21} \cdot \mathbf{a}_2 - \bar{\mathbf{J}}_n(k_\rho\rho_{cn}) \cdot \bar{\mathbf{T}}_{21} \cdot \mathbf{a}_2 \} \\ & = \begin{pmatrix} \sigma_{cn} & 0 \\ 0 & 0 \end{pmatrix} \cdot J_n(k_\rho\rho_{cn}) F_n(z) \bar{\mathbf{T}}_{21} \cdot \mathbf{a}_2, \end{aligned} \quad (25)$$

where we have used the fact that $\partial^2/\partial z^2 = -k_z^2$. Since \mathbf{a}_2 is arbitrary nonzero vector, the two vector equations above can be reduced to the

following system of matrix equations

$$\begin{pmatrix} -H_n^{(2)}(k_\rho \rho_{\text{cn}}) \bar{\mathbf{I}} & J_n(k_\rho \rho_{\text{cn}}) \bar{\mathbf{I}} \\ -\bar{\mathbf{H}}_n^{(2)}(k_\rho \rho_{\text{cn}}) & \bar{\mathbf{J}}_n(k_\rho \rho_{\text{cn}}) + \frac{J_n(k_\rho \rho_{\text{cn}})}{1 - \Upsilon(\omega) k_z^2} \bar{\boldsymbol{\Omega}}(\omega) \end{pmatrix} \times \begin{pmatrix} \bar{\mathbf{R}}_{21} \\ \bar{\mathbf{T}}_{21} \end{pmatrix} = \begin{pmatrix} J_n(k_\rho \rho_{\text{cn}}) \bar{\mathbf{I}} \\ \bar{\mathbf{J}}_n(k_\rho \rho_{\text{cn}}) \end{pmatrix}, \quad (26)$$

where

$$\bar{\boldsymbol{\Omega}}(\omega) = \begin{pmatrix} \sigma_{\text{cn}}(\omega) & 0 \\ 0 & 0 \end{pmatrix}. \quad (27)$$

The solution of these matrix equations is

$$\begin{pmatrix} \bar{\mathbf{R}}_{21} \\ \bar{\mathbf{T}}_{21} \end{pmatrix} = \bar{\mathbf{D}}^{-1} \begin{pmatrix} \bar{\mathbf{J}}_n(k_\rho \rho_{\text{cn}}) + \frac{J_n(k_\rho \rho_{\text{cn}})}{1 - \Upsilon(\omega) k_z^2} \bar{\boldsymbol{\Omega}}(\omega) & -J_n(k_\rho \rho_{\text{cn}}) \bar{\mathbf{I}} \\ \bar{\mathbf{H}}_n^{(2)}(k_\rho \rho_{\text{cn}}) & -H_n^{(2)}(k_\rho \rho_{\text{cn}}) \bar{\mathbf{I}} \end{pmatrix} \times \begin{pmatrix} J_n(k_\rho \rho_{\text{cn}}) \bar{\mathbf{I}} \\ \bar{\mathbf{J}}_n(k_\rho \rho_{\text{cn}}) \end{pmatrix}, \quad (28)$$

where

$$\bar{\mathbf{D}}^{-1} = \left\{ \begin{array}{l} J_n(k_\rho \rho_{\text{cn}}) \bar{\mathbf{H}}_n^{(2)}(k_\rho \rho_{\text{cn}}) - H_n^{(2)}(k_\rho \rho_{\text{cn}}) \bar{\mathbf{J}}_n(k_\rho \rho_{\text{cn}}) \\ - \frac{J_n(k_\rho \rho_{\text{cn}}) H_n^{(2)}(k_\rho \rho_{\text{cn}})}{1 - \Upsilon(\omega) k_z^2} \bar{\boldsymbol{\Omega}}(\omega) \end{array} \right\}^{-1}. \quad (29)$$

Using the Wronskian identity [11], it is possible to simplify (29) as

$$\bar{\mathbf{D}}^{-1} = \begin{pmatrix} \frac{-1}{2\omega\varepsilon/(\pi k_\rho^2 \rho_{\text{cn}}) + A\sigma_{\text{cn}}} & 0 \\ 0 & -\pi k_\rho^2 \rho_{\text{cn}} / 2\omega\mu \end{pmatrix}, \quad (30)$$

where

$$A = \frac{J_n(k_\rho \rho_{\text{cn}}) H_n^{(2)}(k_\rho \rho_{\text{cn}})}{1 - \Upsilon(\omega) k_z^2}. \quad (31)$$

The final solution for the reflection and transmission matrices becomes

$$\bar{\mathbf{R}}_{21} = \frac{[J_n(k_\rho \rho_{\text{cn}})]^2}{1 - \Upsilon(\omega) k_z^2} \begin{pmatrix} \frac{-\sigma_{\text{cn}}}{2\omega\varepsilon/(\pi k_\rho^2 \rho_{\text{cn}}) + A\sigma_{\text{cn}}} & 0 \\ 0 & 0 \end{pmatrix} \quad (32)$$

and

$$\bar{\mathbf{T}}_{21} = \begin{pmatrix} \frac{2\omega\varepsilon}{2\omega\varepsilon + \pi k_\rho^2 \rho_{\text{cn}} A\sigma_{\text{cn}}} & 0 \\ 0 & 1 \end{pmatrix}. \quad (33)$$

We conclude from the final matrices in (32) and (33) that a pure TE mode will pass unaffected through the CNT, which is obvious from the boundary condition (2)–(4). Moreover, we notice also that the off-diagonal terms in the reflection and transmission matrices are zero, indicating that there is no coupling between the TM and TE modes in this structure. Also, we observe that no derivatives of the Bessel and Hankel functions appear in the final solution.

5.2. Outgoing Wave Case

Here, we assume that the n th harmonic of the incident field in Region 1 has the following outgoing wave form (see Figure 3(b))

$$\begin{pmatrix} E_{1z} \\ H_{1z} \end{pmatrix} = H_n^{(2)}(k_\rho \rho) F_n(z) \mathbf{a}_1. \quad (34)$$

This wave can be generated by a source located inside the SWCNT. The total field consists of both the outgoing and reflected standing waves

$$\begin{pmatrix} E_{1z} \\ H_{1z} \end{pmatrix} = J_n(k_\rho \rho) F_n(z) \bar{\mathbf{R}}_{12} \cdot \mathbf{a}_1 + H_n^{(2)}(k_\rho \rho) F_n(z) \mathbf{a}_1. \quad (35)$$

The field transmitted to Region 2 is pure outgoing waveform

$$\begin{pmatrix} E_{2z} \\ H_{2z} \end{pmatrix} = H_n^{(2)}(k_\rho \rho) F_n(z) \bar{\mathbf{T}}_{12} \cdot \mathbf{a}_1. \quad (36)$$

By applying the same procedure of the standing wave case, it is possible to arrive to the following reflection and transmission matrices

$$\bar{\mathbf{R}}_{12} = \frac{[H_n^{(2)}(k_\rho \rho_{\text{cn}})]^2}{1 - \Upsilon(\omega) k_z^2} \begin{pmatrix} \frac{\sigma_{\text{cn}}}{2\omega\varepsilon / (\pi k_\rho^2 \rho_{\text{cn}}) - A\sigma_{\text{cn}}} & 0 \\ 0 & 0 \end{pmatrix} \quad (37)$$

and

$$\bar{\mathbf{T}}_{12} = \begin{pmatrix} \frac{2\omega\varepsilon}{2\omega\varepsilon - \pi k_\rho^2 \rho_{\text{cn}} A\sigma_{\text{cn}}} & 0 \\ 0 & 1 \end{pmatrix}. \quad (38)$$

6. CANONICAL SOLUTION FOR MULTI-WALL CARBON NANOTUBES

We proceed now to the general problem of MWCNTs, each consisting co-centric walls (cylindrical shells) of SWCNT treated as

a homogenized surface using the effective-boundary condition (2)–(4). Each wall can assume an independent chirality. The total structure of the MWCNT will be described then by the sequence $\{(m_i, n_i)\}_{i=1}^N$, where N is the number of walls.

6.1. Standing Wave Problem

Let us assume that a standing wave is incident on the MWCNT. The general structure of the field is both standing and reflected outgoing waves

$$\begin{pmatrix} E_{iz} \\ H_{iz} \end{pmatrix} = \left[H_n^{(2)}(k_\rho \rho) \tilde{\mathbf{R}}_{i,i-1} + J_n(k_\rho \rho) \bar{\mathbf{I}} \right] \cdot \mathbf{a}_i, \quad (39)$$

where $\tilde{\mathbf{R}}_{i,i-1}$ is the generalized reflection matrix seen by the incident standing wave at the interface between media i and $i-1$. Here \mathbf{a}_i is the transmission coefficient of the field in the i th medium. The field in the inner most layer is pure standing wave because the Hankel function is singular at the origin. That is, we set

$$\tilde{\mathbf{R}}_{1,0} = 0. \quad (40)$$

Matching the fields generating the standing wave component in the $(i-1)$ th medium, we get

$$\mathbf{a}_{i-1} = \bar{\mathbf{T}}_{i,i-1} \cdot \mathbf{a}_i + \bar{\mathbf{R}}_{i-1,i} \cdot \tilde{\mathbf{R}}_{i-1,i-2} \cdot \mathbf{a}_i. \quad (41)$$

Similarly, matching the fields generating the outgoing wave component in the i th medium, we obtain

$$\tilde{\mathbf{R}}_{i,i-1} \cdot \mathbf{a}_i = \bar{\mathbf{R}}_{i,i-1} \cdot \mathbf{a}_i + \bar{\mathbf{T}}_{i-1,i} \cdot \tilde{\mathbf{R}}_{i-1,i-2} \cdot \mathbf{a}_i. \quad (42)$$

Solving Equations (41) and (42) simultaneously, we get the following general recursive relations

$$\tilde{\mathbf{R}}_{i,i-1} = \bar{\mathbf{R}}_{i,i-1} + \bar{\mathbf{T}}_{i-1,i} \cdot \tilde{\mathbf{R}}_{i-1,i-2} \cdot \left(\bar{\mathbf{I}} - \bar{\mathbf{R}}_{i-1,i} \cdot \tilde{\mathbf{R}}_{i-1,i-2} \right)^{-1} \cdot \bar{\mathbf{T}}_{i,i-1} \quad (43)$$

and

$$\mathbf{a}_{i-1} = \left(\bar{\mathbf{I}} - \bar{\mathbf{R}}_{i-1,i} \cdot \tilde{\mathbf{R}}_{i-1,i-2} \right)^{-1} \cdot \bar{\mathbf{T}}_{i,i-1} \cdot \mathbf{a}_i. \quad (44)$$

Equations (43) and (44), together with the initial condition (40), are enough to determine the reflection and transmitted fields everywhere. Notice we assume that the incident field vector \mathbf{a}_N is known.

6.2. Outgoing Wave Case

A procedure identical to the standing wave case above can be used to derive the recursive relations for the outgoing wave case. The final results are

$$\tilde{\mathbf{R}}_{i,i+1} = \bar{\mathbf{R}}_{i,i+1} + \bar{\mathbf{T}}_{i+1,i} \cdot \tilde{\mathbf{R}}_{i+1,i+2} \cdot \left(\bar{\mathbf{I}} - \bar{\mathbf{R}}_{i+1,i} \cdot \tilde{\mathbf{R}}_{i+1,i+2} \right)^{-1} \cdot \bar{\mathbf{T}}_{i,i+1} \quad (45)$$

and

$$\mathbf{a}_{i+1} = \left(\bar{\mathbf{I}} - \bar{\mathbf{R}}_{i+1,i} \cdot \tilde{\mathbf{R}}_{i+1,i+2} \right)^{-1} \cdot \bar{\mathbf{T}}_{i,i+1} \cdot \mathbf{a}_i, \quad (46)$$

where obviously we have the following initial condition

$$\tilde{\mathbf{R}}_{N,N+1} = 0. \quad (47)$$

7. SCATTERING OF PLANE WAVES

The general theory presented in the previous sections can be used to construct the response of the CNT to any kind of source excitation. We demonstrate in this section the case when the source lies in the infinity. Therefore, the electromagnetic field impinging on the CNT takes the simple form of plane wave. Assume that this wave is polarized such that the electric field \mathbf{E}^i and the wave vector \mathbf{k}_i are contained in the $\hat{\rho} - \hat{z}$ plane, as shown in Figure 2. The electric field can be written as

$$\mathbf{E}^i = (\hat{\rho} \cos \theta_i + \hat{z} \sin \theta_i) e^{-j\mathbf{k}_\rho \cdot \rho - jk_z z}. \quad (48)$$

where

$$k_\rho = k_0 \sin \theta_i \quad (49)$$

and

$$k_z = -k_0 \cos \theta_i. \quad (50)$$

Here θ_i and ϕ_i are the angles of incidence. We may then write

$$\mathbf{k}_\rho \cdot \rho = k_0 \rho \sin \theta_i \cos(\varphi - \varphi_i). \quad (51)$$

Applying the following well-known cylindrical series expansion identity [11]

$$e^{-jr \cos \varphi} = \sum_{n=-\infty}^{\infty} j^{-n} J_n(r) e^{-jn\varphi}, \quad (52)$$

we write the z -component of the electric field as

$$E_z^i = \sin \theta_i e^{-jk_z z} \sum_{n=-\infty}^{\infty} j^{-n} J_n(k_\rho \rho) e^{-jn(\varphi - \varphi_i)}. \quad (53)$$

The TE^z mode can be treated similarly. The general form of the incident field is written compactly as

$$\begin{pmatrix} E_z^i \\ H_z^i \end{pmatrix} = \sum_{n=-\infty}^{\infty} J_n(k_\rho \rho) F_n(z) \mathbf{a}_N, \quad (54)$$

where

$$F_n(z) = j^{-n} e^{-jn(\varphi - \varphi_i)} e^{-jk_z z}. \quad (55)$$

Here, \mathbf{a}_n denotes the (known) excitation vector amplitude of the combined $\text{TE}^z + \text{TM}^z$ mode. Thus, the response of the CNT to the plane wave incidence is nothing but the superposition of all of the harmonics generated in the canonical solution of the standing wave case.

8. VERIFICATION OF THE MODEL AND RESULTS

8.1. Self-consistency Verification

We have constructed a generalized code for the electromagnetic scattering of multi-layer cylindrical structures. It is expected intuitively that the structure described by the boundary conditions (2)–(4) will approach that of a thin dielectric shell, like the one shown in Figure 4. For the sake of numerical comparison, the surface impedance of the dielectric shell must be converted into a function of the axial conductivity used in the quantum model of the SWCNT. This can be accomplished easily using the relation

$$Z_s = \frac{1}{j\omega(\varepsilon_{\text{cn}} - \varepsilon_0)t} = \frac{1}{\sigma_{\text{cn}}}, \quad (56)$$

where Z_s is the surface impedance, t is the thickness of the dielectric shell, and ε_{cn} is a hypothetical dielectric constant for the SWCNT.

Figure 5 illustrates the comparison described above. The agreement is very good for $t = 0.0001\lambda$. It is readily observed that when the thickness of the dielectric shell increases, discrepancies between the exact and the approximate model show up, as expected. This comparison provides a good self-consistency check on the analytical solution of the boundary conditions (2)–(4). Notice that the same recursive algorithm used to calculate the generalized reflection matrix was employed for *both* the conventional dielectric multilayered problem and the new boundary condition of the MWCNT. Therefore, the consistency of the results serves as a double check on both the multi-layer algorithm and the SWCNT problem.

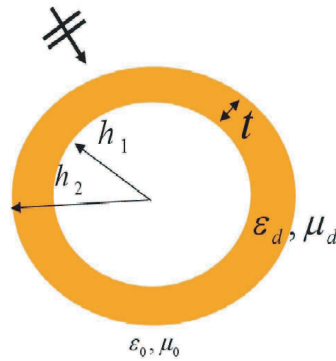


Figure 4. A thin dielectric shell emulates the ideal “zero-thickness” SWCNT with the boundary condition (2)–(4).

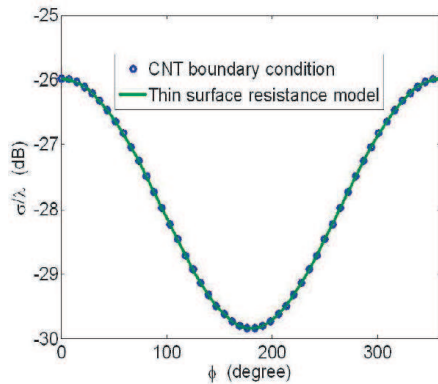


Figure 5. Comparison between the scattering cross section of a SWCNT using the exact solution developed in this paper and the approximation using the thin dielectric shell of Figure 4. The thickness of the shell is $t = 0.0001\lambda$. Here, $\phi_i = 0, \theta_i = 90^\circ$. The shell and the SWCNT are assumed to have a hypothetical dielectric constant of $\epsilon_{cn} = 100 + j10$.

8.2. Scattering Results

In [8], the authors compared the basic solution, obtained using the boundary condition above with Rayleigh scattering data available for SWCNTs, with known crystal structure. Good agreement with empirical data was obtained, giving us confidence that the effective-boundary condition (2)–(4) does capture the physics of carbon nanotubes, at least as long we are concerned with far-field

measurement. Combining this with the verification of the canonical solution of the boundary condition in Sec. 8.1, we proceed now to produce a set of theoretical results for the general case of multi-wall carbon nanotubes.

The effective-boundary conditions in [6] is based on two phenomenological parameters, the overlap energy γ and the relaxation time ν . We assume here that all the tubes have the same values of $\gamma = 3.0$ eV and $\nu = 0.015$ ps, which lie in the expected range at this frequency band and close to the values used in our comparison with the experimental data [8].

The spacing between co-centric tubes in ropes formed typically through self-organization processes was observed to be around around 0.34 nm, which is close to the inter-layer graphene distance around 0.33 nm [3]. From (1), the spacing between two co-centric zigzag nanotubes, say $(n_1, 0)$ and $(n_2, 0)$, is given by $(b_0/2)\pi|n_1 - n_2|$. Using the established value for interatomic distance $b_0 = 0.246$ nm, we readily see that the observed spacing between successive tubes can not be obtained with zigzag structures, but can be easily achieved in armchair tubes $(5n, 5n)$ with arbitrary positive integer n . Therefore, in the remaining parts of this paper, we focus on geometrical models of MWCNTs in which all walls are co-centric armchair tubes with very high aspect ratio.

Figure 6 shows the field scattered by a $(10, 10)$ – $(15, 15)$ – $(20, 20)$

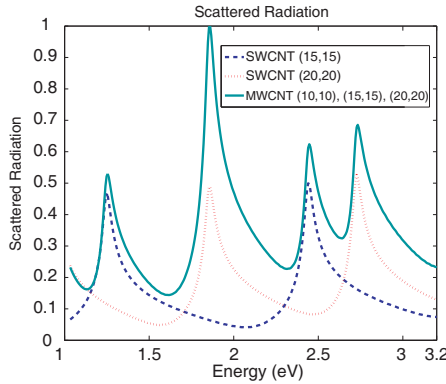


Figure 6. Scattering of the TM^z mode by MWCNT with structure $(10,10)$ – $(15,15)$ – $(20,20)$. Here $\gamma = 3$ eV and $\nu = 0.015$ ps and the effect of spatial dispersion is ignored by setting $\Upsilon(\omega) = 0$. The scattered field is observed at normal incidence with $z = 0$ and $\phi = 0$. Energy is related to frequency by the relation $E = hf$, where h is Planck constant.

MWCNT under normal incidence ($\theta_i = 90^\circ$). In this case, the inner and the outer radii are given by 0.678 nm and 1.356 nm, respectively. The multiple resonances in the MWCNT are due to the interband transitions of the individual tubes. To see this, the scattering results due to SWCNT (15, 15) and (20, 20) are included for comparison. We restrict ourselves here to the energy band shown there for the sake of comparison). All the responses are normalized to the maximum peak calculated in the MWCNT case. The results demonstrate then the effect of the interaction between the walls through the mechanism of electromagnetic scattering and transmission, which has been included in the *generalized* reflection matrix $\tilde{\tilde{\mathbf{R}}}_{i,i+1}$.

The impact of the angle of incidence on the scattering spectrum of the same MWCNT is shown in Figure 7. The results are normalized to the maximum amplitude of the field in the case of normal incidence. As expected, the intrinsic resonance structure exhibited by the nanotube is unaffected by the elevation plane observation, but the power received is drastically reduced when θ approaches zero (grazing angle.)

In Figure 8, we report the bistatic scattering cross section of a double-wall CNT with an inner and outer radii of 26.18 nm and 27.12 nm, respectively. The excitation frequency lies in the ultraviolet band with successive energy levels given by 3.0, 5.0, 8, and 20 eV, corresponding to outer-radius-to-wavelength ratios of 0.065, 0.1097, 0.175 and 0.4374, respectively. For these particular ratios, the modal series expansions converges after few terms. For larger ratios, more terms should be added to insure accurate results. A general rule of thumb is to approximate the number of terms by the larger integer

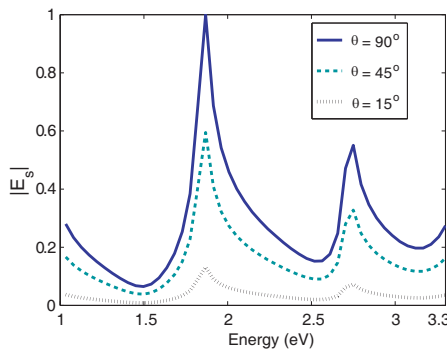


Figure 7. Scattering of the TM^z mode by the same MWCNT in Figure 6. The scattered field is observed at three elevation angles of incidence with $z = 0$ and $\phi_i = 0$.

near to $kb + 5$.

It is noticed that at the shortest wavelength in this example, namely $\lambda = 60$ nm, which corresponds to the energy level 20 eV, the ratio of the operating wavelength to the interatomic spacing $b_0 = 0.246$ nm is given by $b_0/\lambda = 0.0023$, which is still relatively small, justifying the use of the effective-boundary condition in (2)–(4). To demonstrate this, in Figure 9, the spatial dispersion effect, which is included in the factor $\Upsilon(\omega)$ in (4), is taken into consideration and the scattering cross section is compared with the corresponding results for $\theta_i = 45^\circ$ and $E = 20$ eV ($b/\lambda = 0.4374$). As expected, the spatial dispersion effect is still insignificant even in the vacuum ultraviolet regime. However, this conclusion is relevant only to the type of data we are interested with in this paper, which refers mainly to fields measured by *macroscopic* devices that inherently wash out higher-order Floquet modes, which arise from the nonlocal structure of the CNT crystal lattice [9].

Our derivations show that the inclusion of spatial dispersion amounts to introducing a θ_i -dependent factor, namely k_z^2 , into the scattered fields expressions as can be easily seen from (5) and (31). For normal incidence, we find from (50) that $k_z = 0$, which means that the spatial dispersion effect, as revealed by Equation (31), will not manifest itself in the field results. For this reason, the scattering cross

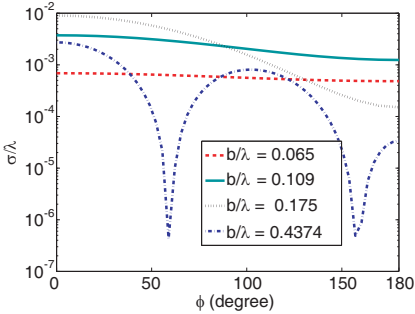


Figure 8. Bistatic scattering cross sections of the TM^z mode of a double-wall CNT with two armchair tubes (395,395) and (400,400). The scattered field is observed at normal incidence with $z = 0$ and $\phi_i = 0$. Here b is the outer radius of the MWCNT.

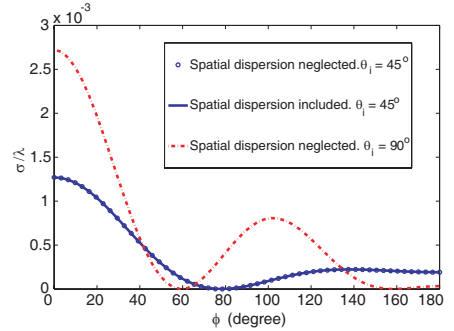


Figure 9. Bistatic scattering cross sections of the TM^z mode of the double-wall CNT described in Figure 8. The scattered field is computed for an operating wavelength $b/\lambda = 0.4374$ and $z = 0$ and $\phi_i = 0$.

section data in Figure 9 were obtained at oblique incidence. Indeed, as shown also in the same figure, the scattering cross section calculated for the normal incidence case $b/\lambda = 0.4374$ in Figure 8 is different from the one calculated in for $\theta_i = 45^\circ$.

Finally, in Figure 10, we study the effect of the outer radius on the scattering cross section of five-wall CNT and a single-wall CNT with the same outer radius, both calculated at the observation location $\phi = 0$ and $z = 0$. The incident field is oblique plane wave given by $\phi_i = 0$ and $\theta_i = 45^\circ$. The operating energy range is from 1 eV to 30 eV with a fixed MWCNT geometry given by $(380, 380) - (385, 385) - (390, 390) - (395, 395) - (400, 400)$. We notice that varying the structure of MWCNT in order to vary the outer radius, while fixing the operating wavelength of the illuminating light, is not a reliable way to see the effect of the radius on the scattering field. This is because for each CNT radius, there corresponds a geometrical structure specified by the integer pair (n, m) . The peculiarity of nanotubes lies in the fact that the geometrical structure varies directly the electronic structure, and hence the electromagnetic response, as can be seen immediately by inspecting the results summarized in Sec. 3.

Since MWCNTs are very small structure, their scattering cross sections are naturally small. However, as our comparison in Figure 10 clearly indicates, the scattered power can be significantly enhanced by increasing the number of walls. Notice that Figure 10 also shows that in this particular frequency band the resonance structure is dominated mainly by the outer nanotube $(380, 380)$.

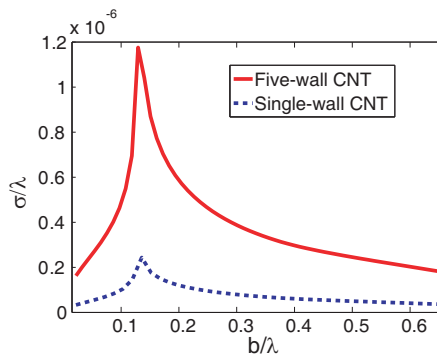


Figure 10. Bistatic scattering cross sections of the TM^z mode of the five-wall CNT $(380, 380) - (385, 385) - (390, 390) - (395, 395) - (400, 400)$. The scattered field is computed at $z = 0$ and $\phi = 0$, for an incident field with $\phi_i = 0$, and $\theta_i = 45^\circ$, under variable operating wavelength λ of the illuminating light. The single-wall CNT in the figure has the same outer layer of the five-wall CNT.

For far-field measurements (e.g., the Rayleigh scattering data included in our comparison with the theoretical model based on the effective-boundary condition (2)–(4) in [8]), we expect that the general model of this paper should provide an insight on the interaction with the electromagnetic field as long as the nanotubes have 1) very high aspect ratio and that 2) the effect of the mutual interaction between the inner walls on the quantum conductivity is ignored. For near-field interactions, however, more careful interpretation of the theoretical model based on the effective-boundary condition may be needed.

9. CONCLUSION

A general algorithm to calculate the scattered fields by arbitrary multi-wall carbon nanotubes was developed starting from an effective-boundary condition. The model takes into consideration the electromagnetic interaction between the walls but ignores any quantum effect of such interactions on the conductivity of each tube. The results of our theoretical model can serve as a basis for the analysis of scattering data collected by macroscopic probes in the far-field zone.

ACKNOWLEDGMENT

This work was partially supported by the Department of Electrical Engineering, University of Mississippi and the National Science Foundation under Grant No. ECS-524293. Also, partial support for this research was provided by ONR Grant No. N00014-07-1-1010, Office of Naval Research, Solid Mechanics Program (Dr. Yapa D. S. Rajapakse, Program Manager).

REFERENCES

1. Iijima, S., “Helical microtubules of graphitic carbon,” *Nature*, Vol. 354, 56–58, 1991.
2. Smalley, R. E., M. S. Dresselhaus, G. Dresselhaus, and P. Avouris, *Carbon Nanotubes: Synthesis, Structure, Properties and Applications*, Springer, 2001.
3. Meyyappan, M., *Carbon Nanotubes: Science and Applications*, CRC Press, 2005.
4. Poole, C. P. and F. J. Owens, *Introduction to Nanotechnology*, Wiley-Interscience, 2003.

5. Slepian, G. Y., et al., "Electronic and electromagnetic properties of nanotubes," *Phys. Rev. B*, Vol. 57, No. 16, 9485–9497, April 1998.
6. Slepian, G. Y., et al., "Electrodynamics of carbon nanotubes: Dynamic conductivity, impedance boundary conditions, and surface wave propagation," *Phys. Rev. B*, Vol. 60, No. 24, 17136–17149, December 1999.
7. Slepian, G. Y., M. V. Shuba, and S. A. Maksimenko, "Theory of optical scattering by achiral carbon nanotubes and their potential as optical nanoantennas," *Phys. Rev. B*, Vol. 73, 195416–195426, May 2006.
8. Mikki, S. M. and A. Kishk, "Theory of optical scattering by carbon nanotubes," *Microwave & Optical Technology Letters*, Vol. 49, No. 10, 2360–2364, October 2007.
9. Mikki, S. M. and A. A. Kishk, "A symmetry-based formalism for the electrodynamics of nanotubes," *Progress In Electromagnetics Research*, PIER 86, 111–134, 2008.
10. Chew, W. C., *Waves and Fields in Inhomogeneous Media*, IEEE Press, re-print edition, 1999.
11. Balanis, C., *Advanced Engineering Electromagnetics*, John Wiley & Sons, 1989.